International Journal of Current Engineering and Technology
E-ISSN 2277 – 4106, P-ISSN 2347 – 5161

Available at https://inpressco.com/category/ijcet

*Research Article*

# Comparative Evaluation of Effective Dielectric Properties of Non-Lead Solid Solutions

**Abhishek Kumar, Ram Kumar, Beauty Kumari, Ankit Kumar, Sandeep Kumar Jha and K. Prasad***

University Department of Physics, T.M. Bhagalpur University, Bhagalpur 812 007, India

Received 01 Jan 2026, Accepted 25 Jan 2026, Available online 31 Jan 2026, **Vol.16, No.1 (Jan/Feb 2026)**

***Abstract***

*Perovskite $ABO_3$ materials have garnered significant attention due to their potential for electronic and microelectronic applications. Lead-based compounds, such as $PbTiO_3$, $Pb(Zr,Ti)O_3$, and $Pb(Mg_{1/3}Nb_{2/3})O_3$, are widely utilized but pose environmental risks, prompting a search for lead-free alternatives. To this end, morphotropic phase boundary composition of Ba-modified $(Bi_{0.5}Na_{0.5})TiO_3$ is considered to be a promising candidate $Ba_{0.06}(Bi,Na)_{0.94}TiO_3$, which shows promising dielectric and piezoelectric properties. In order to further enhance the dielectric characteristics of $Ba_{0.06}(Bi,Na)_{0.94}TiO_3$, the $Ti^{4+}$-ions have been substituted with the pseudo-cation $(Ni_{1/3}^{3+}Nb_{2/3}^{5+})^{4+}$. Accordingly, in this study, lead-free solid solutions of $(1-\phi)Ba_{0.06}Na_{0.47}Bi_{0.47}TiO_3-\phi Ba_{0.06}Na_{0.47}Bi_{0.47}(Ni_{1/3}Nb_{2/3})O_3$ $(0 \le \phi \le 1.0)$ have been synthesized using the solid-state reaction process. Also, the real and imaginary components of permittivity at 1 kHz were analysed as functions of filler $(Ba_{0.06}Na_{0.47}Bi_{0.47}(Ni_{1/3}Nb_{2/3})O_3)$ concentration. The suitability of dielectric mixture equations, including Bruggeman, Furukawa, Rother-Lichtenecker, modified Rother-Lichtenecker, and Knott models, was evaluated. Additionally, a first-order exponential growth model provided an excellent fit to the data ($r^2 > 0.99$).*

***Keywords:*** *Lead free, Solid solution, Complex permittivity, Dielectric mixture equations, Dielectric loss.*

## 1. Introduction

Perovskite $ABO_3$ ferroelectric oxides are highly valued for applications in electronics, microelectronics, pyroelectric and piezoelectric devices. These materials, predominantly lead-based, often incorporate multiple cations at octahedral lattice sites, with heterovalent ions of varying ionic radii, valence states, and polarizabilities enhancing dielectric, electrical, and electromechanical properties. Due to environmental concerns, lead-free ceramic solid solutions have garnered significant attention for their improved dielectric and piezoelectric properties, enabling performance optimization for diverse technological applications [1-3]. Such composite solid solutions provide opportunities to effectively tailor and ultimately optimize their performance according to the requirements. Additionally, determining the true dielectric properties of these materials has attracted widespread global concern in recent years [4-9]. Furthermore, the morphotropic phase boundary composition $Ba_{0.06}(Na_{0.5}Bi_{0.5})_{0.94}TiO_3$ (BNBT) has emerged as a notable lead-free alternative, offering superior dielectric and piezoelectric performance [10,11].

Recent studies have demonstrated the formation of solid solutions involving BNBT with $Ba(Fe_{0.5}Nb_{0.5})O_3$ [12], $Ba(Fe_{0.5}Ta_{0.5})O_3$ [13], and $NaNbO_3$ [14,15], yielding materials with exceptionally high dielectric constants. Additionally, pseudo-cation substitution, such as $(Mg_{1/3}Nb_{2/3})^{4+}$, has been shown to influence phase transition behavior in BNBT systems [16,17]. In this work, the dielectric performance of BNBT is further enhanced by substituting $Ti^{4+}$ with the pseudo-cation $(Ni_{1/3}^{3+}Nb_{2/3}^{5+})^{4+}$.

Accordingly, solid solutions of $(1-\phi)Ba_{0.06}Na_{0.47}Bi_{0.47}TiO_3-\phi Ba_{0.06}Na_{0.47}Bi_{0.47}(Ni_{1/3}Nb_{2/3})O_3$(BNBT/BNBNN; $0 \le \phi \le 1.0$) were synthesized via the conventional mixed-oxide route and systematically characterized using X-ray diffraction, scanning electron microscopy, and dielectric measurements. The dielectric constant and loss factor were evaluated utilizing various dielectric mixture equations, including perturbation expansion, variational approaches, and effective medium approximations, to determine the most suitable model across the full range of inclusion material volume fractions.

## 2. Experimental details

Lead-free solid solutions of $(1-\phi)$BNBT–$\phi$BNBNN ($0 \le \phi \le 1.0$) were synthesized via the conventional mixed

*Corresponding author: K. Prasad
DOI: https://doi.org/10.14741/ijcet/v.16.1.3

oxide method using analytical reagent-grade precursors: $BaCO_3$, $Na_2CO_3$, $Bi_2O_3$, $TiO_2$, NiO, and $Nb_2O_5$ in stoichiometric proportions. Calcination conditions were optimized to 1140°C/4 hours for BNBT and 1100°C/4 hours for the remaining compositions. These calcined powders were then pressed into cylindrical pellets having a diameter of 10 mm and a thickness of ~1.5 mm under a pressure (uniaxial) of 6 tons, using polyvinyl alcohol as a binder. These green pellets were subsequently sintered at 1160°C/3 hours for BNBT and at 1120°C/4 hours for other compositions in different crucibles covered with platinum foil. Phase formation was analyzed using X-ray diffraction (XRD) on a Bruker D8 Advance diffractometer with $CuK_\alpha$ radiation (λ = 1.5405 Å) over a 2θ range of 20°–70°. Unit cell parameters, space group, and crystallographic details (hkl values) were refined using the Rietveld method via FullProf software. Fractured surfaces of sintered specimens were examined for surface morphology using a scanning electron microscope (Zeiss EVO 18). To ensure moisture-free surfaces, all samples were oven-dried at 80°C for 3 hours before applying silver paste (air-dried) to both flat surfaces for carrying out the dielectric measurements. Room-temperature dielectric properties were measured using an LCR Hi-Tester (Japan, HIOKI 3532-50) attached to a computer for data acquisition.

## 3. Theoretical models

The accurate determination of the filler-concentration dependent effective permittivity (dielectric constant, $\varepsilon'_{eff}$) and loss factor ($\varepsilon''_{eff}$) of solid solutions is critical for material design [18]. Numerous theoretical models, including those proposed by Maxwell-Wagner, Skipetrov, Knott, Furukawa, Rother-Lichtenecker, Bruggeman, Hashin-Shtrikman, Cuming, Taylor, Wiener, Poon-Shin, Lewin, Jayasundere-Smith, Sillars, and modified Cule-Torquato, have been employed to estimate $\varepsilon'_{eff}$ for a range of composite systems [19–21]. The models utilized in this study are detailed below:

(a) Bruggeman equation (BE):

$$\varepsilon'_{eff} = \varepsilon'_m \left[1 + \frac{\varphi_f(\varepsilon'_f - \varepsilon'_m)}{\varepsilon'_m + n(1-\varphi_f)(\varepsilon'_f - \varepsilon'_m)}\right] \quad (1)$$

Here, subscripts $f$ and $m$ denote filler and matrix, respectively, and $n$ is an adjustable parameter (shape dependent) based on data variations.

(b) Furukawa equation (FE)/Effective medium theory (EMT)/Webman theory

$$\varepsilon'_{eff} = \varepsilon'_m \left[\frac{1+2\varphi_f\{(\varepsilon'_f - \varepsilon'_m)/(\varepsilon'_f + 2\varepsilon'_m)\}}{1-\varphi_f\{(\varepsilon'_f - \varepsilon'_m)/(\varepsilon'_f + 2\varepsilon'_m)\}}\right] \quad (2)$$

(c) Cuming model/Rother-Lichtenecker equation (RLE):

$$\varepsilon'_{eff} = exp(\sum_i \varphi_i \, ln \, \varepsilon'_i) \quad (3)$$

where $\phi_i$ and $\varepsilon'_i$, respectively represent the volume fraction, and dielectric constant of the $i^{th}$ component.

(d) Modified Rother-Lichtenecker equation (mRLE):

$$\varepsilon'_{eff} = exp[\, ln \, \varepsilon'_m + \varphi_f(1-k) \, ln(\varepsilon'_f/\varepsilon'_m)] \quad (4)$$

Here, $k$ is a shape-dependent parameter. Equations (3) and (4) are variations of the logarithmic mixing law applicable to statistical or chaotic mixtures.

For solid solutions, few models account for the filler-concentration dependence of $\varepsilon''_{eff}$. One notable equation, introduced by Bruggeman [22], offers an approach to incorporate all available models for $\varepsilon'_{eff}$ into its framework for comparison with experimental data.

$$\varepsilon''_{eff} = \frac{\varepsilon''_m[(\varepsilon'_f - \varepsilon')(\varepsilon'_f + 2\varepsilon'_m)\varepsilon']}{[(\varepsilon'_f - \varepsilon'_m)(\varepsilon'_f + 2\varepsilon')\varepsilon'_m]} + \varepsilon''_f \frac{3(\varepsilon' - \varepsilon'_m)\varepsilon'}{(\varepsilon'_f - \varepsilon'_m)(\varepsilon'_f + 2\varepsilon')} \quad (5)$$

In this work, Equations (1)–(4) were applied in Equation (5) to predict $\varepsilon''_{eff}$ of (1-$\phi$)BNBT–$\phi$BNBNN (0 ≤ $\phi$ ≤ 1.0) solid solutions and compared with experimental measurements.

## 3. Results and discussion

Figure 1 displays the Rietveld-refined XRD profiles of (1-$\phi$)BNBT–$\phi$BNBNN solid solutions for 0 ≤ $\phi$ ≤ 1.0. The presence of sharp, single-phase peaks without any additional reflections from constituent oxides or carbonates confirms the favorable formation of homogeneous solid solutions. This indicates the gross incorporation of the pseudo-cation $(Ni^{3+}_{1/3}Nb^{5+}_{2/3})^{4+}$ into the BNBT matrix. XRD analysis reveals that the BNBT ($\phi$ = 0) exhibits a monoclinic unit cell structure with

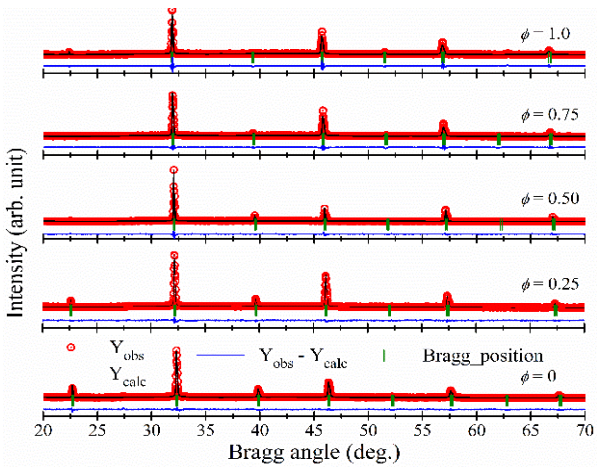


**Fig. 1** Room temperature XRD profiles (Rietveld refined) of BNBT/BNBNN solid solutions. Symbols represent the observed data points and the solid lines their Rietveld fit.

**Table 1.** The lattice information of BNBT/BNBNN solid solutions at room temperature.

| Solid solutions | $\phi = 0$ | $\phi = 0.25$ | $\phi = 0.50$ | $\phi = 0.75$ | $\phi = 1.0$ |
|---|---|---|---|---|---|
| $a$ (Å) | 3.99 | 3.93 | 3.94 | 3.95 | 3.9668 |
| $b$ (Å) | 3.86 | 3.93 | 3.94 | 3.95 | 3.9668 |
| $c$ (Å) | 3.29 | 2.78 | 2.79 | 2.80 | 3.9662 |
| $\beta$ (°) | 102.9 | 90.00 | 90.00 | 90.00 | 90.00 |

the space group of $P2/m$, whereas BNBNN ($\phi$ = 1.0) adopts a tetragonal (pseudo-cubic) structure having the space group of $P4/mmm$. Variations in peak intensities and Bragg positions are evident across compositions, reflecting changes in lattice parameters (as shown in Table 1) and crystal symmetry due to the inclusion of the pseudo-cation $(Ni^{3+}_{1/3}Nb^{5+}_{2/3})^{4+}$. Rietveld refinement of intermediate compositions ($\phi$ = 0.25, 0.50, and 0.75) indicates that these solid solutions crystallize in a tetragonal phase having the $P4/mmm$ space group. Thereby, the partial substitution of $Ti^{4+}$ by $(Ni^{3+}_{1/3}Nb^{5+}_{2/3})^{4+}$ is accountable for altering the fundamental lattice structure of the solid solutions.

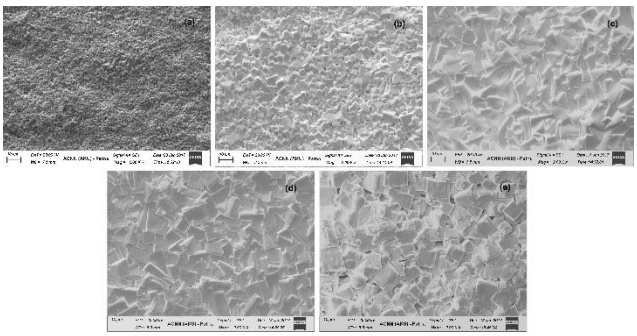

**Fig. 2** SEM micrographs of BNBT/BNBNN solid solutions (scale: 10 μm).

Figure 2 presents scanning electron microscopy images (SEM) of the fractured surfaces of (1-$\phi$) BNBT–$\phi$BNBNN solid solutions ($0 \le \phi \le 1.0$). The micrographs reveal densely packed, nearly cuboidal grains with varying sizes distributed uniformly across all compositions. The absence or minimal presence of voids indicates the high density of the synthesized solid solutions. The mean grain sizes for compositions with $\phi$ = 0, 0.25, 0.50, 0.75, and 1.0 were measured as 120.7 nm, 156.6 nm, 191.8 nm, 149.0 nm, and 177.8 nm, respectively. These results demonstrate significant changes in grain size and morphology with increasing $\phi$, suggesting a strong dependence of microstructural evolution on the composition of BNBT/BNBNN solid solutions.

Figure 3 (a) and (b) depict the dependence of real ($\varepsilon'$) and imaginary ($\varepsilon''$) parts of the room temperature dielectric constant at 1 kHz on BNBNN content ($\phi$) in BNBT/BNBNN solid solutions. The experimental data (symbols) are shown alongside fitted curves obtained from different predictive models. An increase in $\varepsilon'_{eff}$ and $\varepsilon''_{eff}$ values is observed, with $\varepsilon'$ rising from 328 to 801 and $\varepsilon''$ increasing significantly from 39 to 1554 as the BNBNN content in the BNBT matrix increases. The Bruggeman Equation (BE) model exhibits excellent concurrence with the experimental findings for both $\varepsilon'$ and $\varepsilon''$ across the entire range of $\phi$. This strong correlation is attributed to the inclusion of the adjustable shape-dependent parameter ($n$), which is optimized to 0.9 for the current study. In contrast, other predictive models such as the Furukawa Equation (FE), Rother-Lichtenecker Equation (RLE), and modified Rother-Lichtenecker Equation (mRLE) fail to adequately describe the experimental $\varepsilon'$–$\phi$ and $\varepsilon''$–$\phi$ trends.

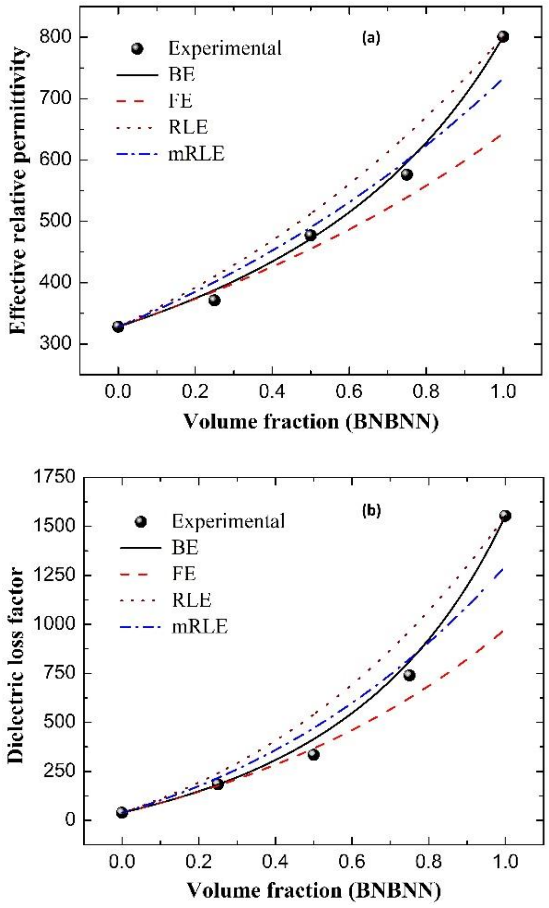


**Fig. 3** Composition ($\phi$) dependent variation of (a) effective dielectric constant, and (b) dielectric loss factor of BNBT/BNBNN solid solutions at 1 kHz and room temperature.

The as obtained experimental data of $\varepsilon'$ and $\varepsilon''$ of BNBT/BNBNN solid solutions could not be accurately described by any of the conventional mixture equations, except for the Bruggeman Equation (BE), which showed limited agreement. To address this discrepancy, a novel model for the filler (BNBNN) concentration-dependent variation of $\varepsilon'$ and $\varepsilon''$ was proposed [20,23,24]. This model, a first-order exponential growth function, is expressed as:

$$Y = Y_o + A\,exp(\varphi/t) = Y_o + A\,exp(\beta\varphi) \quad (6)$$

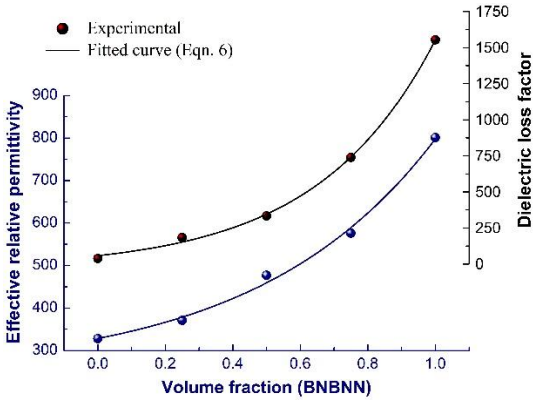


**Fig. 4** Variation of room temperature dielectric constant and dielectric loss factor of BNBT/BNBNN solid solutions at 1 kHz along with the fitted curves; model Eq. (6).

**Table 2.** Fitted parameters from Eq. (6) for the real and imaginary components of the dielectric constant of BNBT/BNBNN solid solutions, measured at 1 kHz and room temperature.

| Equations → | Exponential growth function (Eq. 6) | | | |
|---|---|---|---|---|
| Parameters ↓ | $Y_o$ | $A$ | $t$ | $r^2$ |
| $\varepsilon'$ | 245.61758 | 82.64998 | 0.52649 | 0.99225 |
| $\varepsilon''$ | -32.00813 | 89.97453 | 0.3486 | 0.99797 |

The parameters $Y_o$, $A$, $t$, or $\beta$ (=1/$t$), and the coefficient of determination ($r^2$) for both $\varepsilon'$ and $\varepsilon''$ were derived through curve fitting, as summarized in Table 2. The results demonstrate excellent agreement with $r^2$ > 0.99, indicating the model's robustness in describing the experimental data. Here, $Y_o$+$A$ corresponds to $\varepsilon'$ or $\varepsilon''$ at saturation, while $\beta$ is interpreted as the growth parameter that depends upon the dielectric constant of the filler. Fig. 4 illustrates the experimental data and fitted curves for ε′ and ε″ based on Eq. (6). The excellent fit ($r^2$ > 0.99) highlights the model's applicability to BNBT/BNBNN solid solutions. Notably, the values of $\beta$ vary with different combinations of ceramics, likely due to differences in densification behavior as denser ceramic particles replace lighter ones with increasing volume fractions. The variation in $\beta$ may also be linked to the relative permittivity of the ceramic particles, serving as a calibration parameter to describe the sharpness or flatness of the variation. This study suggests that $\beta$ offers valuable insights into the material's microstructural and dielectric characteristics, making it a potentially useful parameter for future investigations of ceramic-ceramic composites.

## 4. Conclusion

Lead-free solid solutions of $(1\text{-}\phi)Ba_{0.06}(Na,Bi)_{0.94}TiO_3$-$\phi Ba_{0.06}(Na,Bi)_{0.94}(Ni_{1/3}Nb_{2/3})O_3$ ($0 \le \phi \le 1.0$) were fabricated using the solid-state reaction process. The dielectric properties, specifically the real ($\varepsilon'$) and imaginary ($\varepsilon''$) parts of the dielectric constant, were found to increase consistently with the filler (BNBNN) concentration. To evaluate the suitability of dielectric mixture equations for predicting the behaviour of the composite, four models were analysed. Among these, the Bruggeman equation demonstrated excellent coherence with the experimental data, exhibiting minimal deviations across the whole range of volume fractions for both $\varepsilon'$ and $\varepsilon''$. Furthermore, a first-order exponential growth type model was proposed to describe the filler-concentration-dependent variation of the dielectric constant. This model demonstrated an exceptional fit to the experimental data, achieving a coefficient of determination ($r^2$) greater than 0.99, thereby validating its applicability for accurately characterizing the dielectric behaviour of these solid solutions.

## References

[1] Z. Li, Q. Yang, C. Wang, J. Zhang, Z. Wang, B. Gao, Z. Li, Z. Wang, X. Yan, T. Ai, D. Wang, Y. Niu, A brief review of sodium bismuth titanate-based lead-free materials for energy storage: solid solution modification, metal/metallic oxide doping, defect engineering and process optimizing, Crystals 13 (2023) 295.

[2] L. Chen, H. Liu, H. Qi, J. Chen, High-electromechanical performance for high-power piezoelectric applications: fundamental, progress, and perspective, Prog. Mater. Sci. 127 (2022) 100944.

[3] P.K. Panda, B. Sahoo, PZT to lead free pieo ceramics: A review, Ferroelectr. 474 (2015) 128-143.

[4] A. Kumar, Subrato, K. Prasad, Electrical properties and electromagnetic radiation characteristics of cement/$Ba_{0.06}Bi_{0.47}Na_{0.47}TiO_3$ composites, Process. Appln. Ceram. 18(2) (2024) 186-195.

[5] A. Kumar, K. Prasad, Impact-based energy harvesting characteristics of Cement/Pb$(Zr_{0.52}Ti_{0.48})O_3$ composites, Ferroelectr. 613(1) (2023) 148-159.

[6] A. Kumar, K. Prasad, effective complex permittivity of random composite media: PVDF/$(Na_{1/2}Bi_{1/2})TiO_3$, Mater. Sci. Forum 1074 (2022) 47–52.

[7] A. Kumar, A. Kumar, K. Prasad, Evaluation of $(Na_{1/2}Bi_{1/2})TiO_3$/PVDF piezocomposites for mechanical energy harvesting, Solid State Sci. 121 (2021) 106729 (8 pages).

[8] A. Kumar, A. Kumar, K. Prasad, Energy harvesting from ceramic/blended polymer nanocomposites: $Ba_{0.85}Ca_{0.15}Zr_{0.10}Ti_{0.90}O_3$/Polyvinylidene fluoride–Polytetrafluoroethylene, Phys. Status Solidi A: Appln. Mater. Sci. 218(20) (2021) 2100382.

[9] A. Kumar, A. Kumar, K. Prasad, Power generation characteristics of $0.50(Ba_{0.7}Ca_{0.3})TiO_3$–$0.50Ba(Zr_{0.2}Ti_{0.8})O_3$/PVDF nanocomposites under impact loading, J. Mater. Sci.: Mater. Electron. 31 (2020) 12708–12714.

[10] T. Takenaka, K. Sakat, Piezoelectric properties of $(Bi_{0.5}Na_{0.5})TiO_3$-based ceramics. Ferroelectr. 106 (1990) 375-380.

[11] J. Lv, Q. Li, Y. Li, M. Tang, D. Jin, Y. Yan, B. Fan, L. Jin, G. Liu, Significantly improved energy storage performance of NBT-BT based ceramics through domain control and preparation optimization, Chem. Engg. J. Part I 420 (2021) 129900.

[12] S.K. Roy, S.N. Singh, S.K. Mukherjee, K. Prasad, Structure and dielectric studies of (1-

x)$Ba_{0.06}(Na_{0.5}Bi_{0.5})_{0.94}TiO_3$-x$Ba(Fe_{0.5}Nb_{0.5})O_3$ lead-free ceramics, Process. Appln. Ceram. 13(4) (2019) 418–426.

[13] S.K. Roy, S.N. Singh, S.K. Mukherjee, K. Prasad, $Ba_{0.06}(Na_{1/2}Bi_{1/2})_{0.94}TiO_3$-$Ba(Fe_{1/2}Ta_{1/2})O_3$: Giant permittivity lead-free ceramics, J. Mater. Sci.: Mater. Electron. 28 (2017) 4763-4771.

[14] S.K. Roy, S. Chaudhuri, R.K. Kotnala, D.K. Singh, B.P. Singh, S.N. Singh, K.P. Chandra, K. Prasad, Dielectric and Raman studies of $Ba_{0.06}(Na_{1/2}Bi_{1/2})_{0.94}TiO_3$-$NaNbO_3$ ceramics, Mater. Sci.-Poland 34 (2016) 437-445.

[15] S.K. Roy, S.N. Singh, K. Prasad, Structure, microstructure and infrared studies of $Ba_{0.06}(Na_{1/2}Bi_{1/2})_{0.94}TiO_3$-$NaNbO_3$ ceramics, AIP Conf. Proc. 1728 (2016) 020217-4.

[16] E.A. Zereffa, A. Prasad Rao, Effect of simultaneous substitution of magnesium and niobium on dielectric properties and phase transition temperature of bismuth sodium barium titanate ceramics, Mater. Sci.-Poland 31 (2013) 201-210.

[17] A. Prasad, R.K. Mishra, K.P. Chandra, K. Prasad, Structural and electrical properties of $(Bi,Na)_{0.94}Ba_{0.06}Ti_{1-x}(Mg_{1/3}Nb_{2/3})_xO_3$ ceramics, Process. Appln. Ceram. 12(4) (2018) 383–393.

[18] J.D. González-Teruel, S.B. Jones, F. Soto-Valles, R. Torres-Sánchez, I. Lebron, S.P. Friedman, D.A. Robinson, Dielectric spectroscopy and application of mixing models describing dielectric dispersion in clay minerals and clayey soils, Sensors 20(22) (2020) 6678.

[19] A. Prasad, K. Prasad, Effective permittivity of random composite media: A comparative study, Physica B: Conden. Matter 396(1) (2007) 132-137.

[20] Z. Ahmad, A. Prasad, K. Prasad, A comparative approach to predicting effective dielectric, piezoelectric and elastic properties of PZT/PVDF composites, Physica B: Conden. Matter 404(20) (2009) 3637-3644.

[21] H. Ranjan, U.K. Mahto, K.P. Chandra, A.R. Kulkarni, A. Prasad, K. Prasad, Electrical and magnetic properties of 0-3 $Ba(Fe_{1/2}Nb_{1/2})O_3$/PVDF composites, J. Adv. Dielectr. 7(6) (2017) 1750036 (11 pages).

[22] X.X. Wang, K.H. Wang, X.G. Tang, H.L.W. Chan, Dielectric characteristics and polarization response of lead-free ferroelectric $(Bi_{0.5}Na_{0.5})_{0.94}Ba_{0.06}TiO_3$–P(VDF-TrFE) 0-3 composites, Solid State Commun. 130 (2004) 695-699.

[23] A.K. Roy, Z. Ahmad, A. Prasad, K. Prasad, Concentration dependent dielectric properties of Barium Titanate/Polyvenylidene Fluoride (PVDF) and $(Bi_{0.5}Na_{0.5})_{0.94}Ba_{0.06}TiO_3$/Poly(VDF-TrFE) composite, Adv. Mater. Res. 1(4) (2012) 285-297.

[24] K.P. Chandra, R. Singh, A.R. Kulkarni, K. Prasad, Dielectric relaxation in 0-3 PVDF-$Ba(Fe_{1/2}Nb_{1/2})O_3$ composites, AIP Conf. Proc. 1728 (2016) 020638-4.